Band structure and Fermi surface nesting in $LaSb_2$

Evan O'Leary,[1,2] Lin-Lin Wang,[1,2] Yevhen Kushnirenko,[1,2] Benjamin Schrunk,[1,2] Andrew Eaton,[1,2] Paula Herrera-Siklody,[1] Sergey L. Bud'ko,[1,2] Paul C. Canfield,[1,2,*] and Adam Kaminski[1,2,†]

[1]*Department of Physics and Astronomy, Iowa State University, Ames, Iowa 50011, USA*

[2]*Ames National Laboratory, U.S. Department of Energy, Ames, Iowa 50011, USA*

(Received 26 March 2024; revised 14 May 2024; accepted 28 June 2024; published 17 July 2024)

We use high-resolution angle-resolved photoemission spectroscopy (ARPES) and density functional theory (DFT) to investigate the electronic structure of the charge density wave (CDW) system $LaSb_2$. This compound is among an interesting group of materials that manifests both a CDW transition and lower temperature superconductivity. We find the DFT calculations to be in good agreement with our ARPES data. The Fermi surface of $LaSb_2$ consists of two small hole pockets close to Γ and four larger pockets near the Brillouin zone boundary. The key features of the Fermi surface do not vary significantly with temperature. A saddle point is present at −0.19 eV below the Fermi level at Γ. Saddle points in the band structure have more pronounced effects on materials properties when they are located closer to the Fermi level, making doped $LaSb_2$ compounds a potential interesting subject of future research. Multiple peaks are present in the generalized, electronic susceptibility calculations, indicating the presence of three possible nesting vectors. We were not able to detect any signatures of the CDW transition at 355 K down to the lowest temperature of 7 K, pointing to the subtle nature of this transition. This is unusual, given that such a high transition temperature is expected to be associated with the presence of a large CDW gap. This is confirmed through investigation of the Fermi surface and through analysis of momentum distribution curves. It is possible that changes are subtle and occur below current sensitivity of our measurements.

DOI: 10.1103/PhysRevB.110.035145

I. INTRODUCTION

The rare-earth diantiminides have been known crystallographically since 1969, but until the systematic growth of single crystals from excess Sb solution, little was known about their physical properties [1–3]. The RSb_2 (R = La–Sm) series was initially studied in single-crystal form, producing subsequent papers studying effects of doping, pressure, and high magnetic field [4,5]. The crystal structure of $LaSb_2$ is orthorhombic and highly layered, with a minor difference between the in-plane lattice constants [6]. $LaSb_2$ can be described as metallic-micaceous in that it readily exfoliates into highly malleable 2D-like sheets [4]. As such, it is very well suited for ARPES experiments. $LaSb_2$ is part of a special group of materials that exhibit superconductivity and charge density wave (CDW) order [6–8]. The coexistence of superconductivity and CDW order have been studied previously in the transition metal dichalcogenide systems $NbSe_2$, $1T - TaS_2$, and $TaSe_2$ [9–11]. Similarly to $LaSb_2$, they are also highly layered. The superconducting transition in $LaSb_2$ occurs at $T_c = 1.2$ K, while two separate CDW transitions are proposed at 355 K and below 200 K [6–8,12]. Another interesting feature of $LaSb_2$ is the large, linear magnetoresistance that does not saturate at high fields [6].

The transport properties of $LaSb_2$ have been extensively studied. The resistivity of $LaSb_2$ is expected to be anisotropic based on the crystal structure. This was confirmed by single-crystal four-probe resistivity measurements [4]. A more recent study claims that the single-crystal $LaSb_2$ has an isotropic resistivity tensor [13]. The unexpected isotropic resistivity tensor is explained by crystal imperfections. Further, scanning tunneling microscopy measurements show that $LaSb_2$ enters a superconducting state at $T_c \approx 1.2$ K, while more recent resistivity measurements place the transition at $T_c \approx 0.4$ K [5,6]. Unfortunately, this temperature is not easily attainable for ARPES measurements.

Several experiments have attempted to verify the CDW state in $LaSb_2$ below 355 K, with evidence remaining fairly elusive [5,6,8,13]. Resistivity data indicates CDW order in $LaSb_2$ through a dip and a hysteresis of 2 K around 350 K [5,8]. The CDW transition is more apparent and shifts to roughly 150 K upon substitution of La with Ce to around 50% [8]. The sharpening of the hysteresis is suspected to be caused by the introduced disorder in the system. Single crystal x-ray diffraction on pure $LaSb_2$ showed peaks where systematic absences were expected, indicating a mixing of the a and b directions potentially as a result of twinning or stacking faults [13]. This is potential evidence that innate disorder in pure $LaSb_2$ may be the origin of the CDW state. The resistivity hysteresis may also be enhanced by applied pressure, increasing to a width of 50 K, and shifting to lower temperature until it is completely suppressed at 6–7 kbar [5,14].

Another interesting property of $LaSb_2$ is the large, linear magnetoresistance that does not saturate up to a field of 45 T [6,8,14]. It is speculated that scattering rate variations with

*Contact author: canfield@ameslab.gov
†Contact author: adamkam@ameslab.gov

applied magnetic field are the cause of the linear magnetoresistance [15]. This is based on the minor changes seen in the optical reflectivity when the magnetic field is varied. The large linear magnetoresistance makes $LaSb_2$ a good candidate for magnetic field sensors [16].

The electronic band structure of $LaSb_2$ has been previously investigated using de Haas-van Alphen (dHvA) technique, ARPES, and density functional theory calculations [17,18]. The dHvA measurements showed a quasi-two-dimensional Fermi surface with two nearly cylindrical extremal orbits and one small ellipsoidal orbit [17]. These measurements were in rough agreement with the calculated Fermi surface. The density functional theory (DFT) calculations seemed to agree well with the observed Fermi surface. The latest ARPES measurements showed that $LaSb_2$ has multiple topological nodal points, lines, and surfaces, including eightfold degenerate nodal points [19]. The multiple topological nodal structure is cited as another potential explanation of the large linear magnetoresistance in this material. We are not aware of any previous measurements of the band structure near the CDW transition at 355 K, motivating this paper.

II. METHODS

Large single crystals of $LaSb_2$ were grown out of antimony flux [2,4,5]. Elemental La (99.99+ Ames Laboratory) and Sb (99.999+ Alfa Aesar) were combined in the ratio of La_5Sb_{95} and placed into the bottom part of a 2 ml Canfield Crucible set (CCS) [20,21]. The CCS was sealed into an amorphous silica tube with silica wool on top of the CCS to act as a cushion during the decanting process. The sealed ampule was heated over 3 h to 1100 °C, held at 1100 °C for 5 h, and then cooled to 1000°C over 1 h. After sitting at 1000 °C for 5 h, the ampoule was cooled to 675 °C over 99 h. Upon reaching 675 °C, the ampule was removed from the furnace and decanted in a laboratory centrifuge [22]. After cooling to room temperature, the ampule was opened, revealing large, sometimes crucible limited crystals of $LaSb_2$.

The ARPES measurements were performed by cleaving $LaSb_2$ *in situ* at base pressure lower than 5×10^{-11} Torr. The 330 K and 360 K data were measured from the same sample, which was cleaved at 330 K. The 7 K data was measured and cleaved at 7 K. The temperature of the sample was determined by using Cernox sensor calibrated at a sample position. A Scienta DA30 analyzer was used in conjunction with a tunable, picosecond Ti:Sapphire laser and fourth-harmonic generator operating at 6.7 eV [23]. A second, fixed wavelength laser was also used in conjunction with the fourth harmonic generator and operated at 7 eV. All data was acquired using vertical polarization. The chemical potential was determined by measuring a polycrystalline Cu reference sample that was in electrical contact with the $LaSb_2$, and fitting a Fermi function to the data. One data set, shown in Fig. 1(c), was taken while applying a −7 V bias potential to the sample. A copper disk of radius 1.2 cm was electrically isolated from the rest of the ARPES system and the potential was supplied by a DC Power Supply 9116 from BK Precision directly to the disk. This technique has been tested and theoretically analyzed, where for a comparable setup there were little to no distortions when the applied bias is less than 10 V [24].

Band structures of $LaSb_2$ have been calculated using DFT [25,26] using PBE [27] exchange-correlation functional with spin-orbit coupling (SOC) and experimental lattice parameters. DFT calculations were performed in VASP [28,29] with a plane-wave basis set and projector augmented-wave [30] method. We used the primitive unit cell of 12 atoms with a Γ-centered Monkhorst-Pack [31] (11 x 11 x 3) k-point mesh and a Gaussian smearing of 0.05 eV to converge charge density. A tight-binding model based on maximally localized Wannier functions [32–34] was constructed to closely reproduce the bulk band structure including SOC in the range of $E_F \pm 1$eV with La sdf and Sb p orbitals. Then the spectral functions and Fermi surface of a semi-infinite $LaSb_2$ (001) surface were calculated with the surface Green's function methods [35–38] as implemented in WANNIERTOOLS [39]. The real part of the susceptibility function has been calculated on a dense k-point mesh of (160 x 160 x 40) to study Fermi surface nesting.

III. RESULTS AND DISCUSSION

Density functional theory calculations are presented in Fig. 1. The crystal structure and possible surface terminations are shown in Fig. 1(a). To confirm the CDW transition in our samples, we provide resistivity data in Fig. 1(d), which shows a kink at 355 K. In Figs. 1(e), 1(g) and 1(h), we show DFT calculations cutting along the X-Γ-X direction for the three possible terminations. The ARPES data in Fig. 2(e) along the X-Γ-X direction shows a conduction band which goes down in energy to −0.19 eV. The DFT calculations for terminations 2 and 3 differ from the ARPES data as they have conduction bands that bottom out in energy around 0.08 eV. There are also two additional bands which appear in the DFT calculations, which are not seen in ARPES. For these reasons, we conclude the surface termination is at the $(LaSb)_2$ layer (T1), shown in Fig. 1(a). Comparison of Figs. 1(b) and 1(c) reveals that two small round pockets appear in both the DFT calculations and ARPES data and have very similar shape. There are multiple outer pockets predicted by the calculations, which are also seen in the ARPES data. They are similar in shape and location, but ARPES intensity fades out in the upper corner of Fig. 1(c). The ARPES data appear to have good agreement with the DFT calculations. The DFT calculations also have good agreement with previously published ARPES data and theoretical calculations [12,17].

Saddle points points in the energy dispersion of three-dimensional materials produces a divergence in the density of states (DOS), and causes the derivative of the DOS to be non-continuous, known as a van Hove singularity. When saddle points in the electronic structure are near or coincide with the Fermi energy, materials may present with interesting properties such as superconductivity, magnetism, or charge and spin density waves [40,41]. It is general practice to try and tune the location of the van Hove singularity to a lower binding energy. This can be accomplished either via doping or other mechanical methods as in twisted graphene [40,41]. In Fig. 2, we present ARPES data that reveals the presence of a saddle point located at Γ. The inner pockets discussed previously that are closest to Γ make up the upwards dispersion of the saddle point. The dispersions across the pockets for several cuts are shown in Figs. 2(c)–2(g), showing an upward

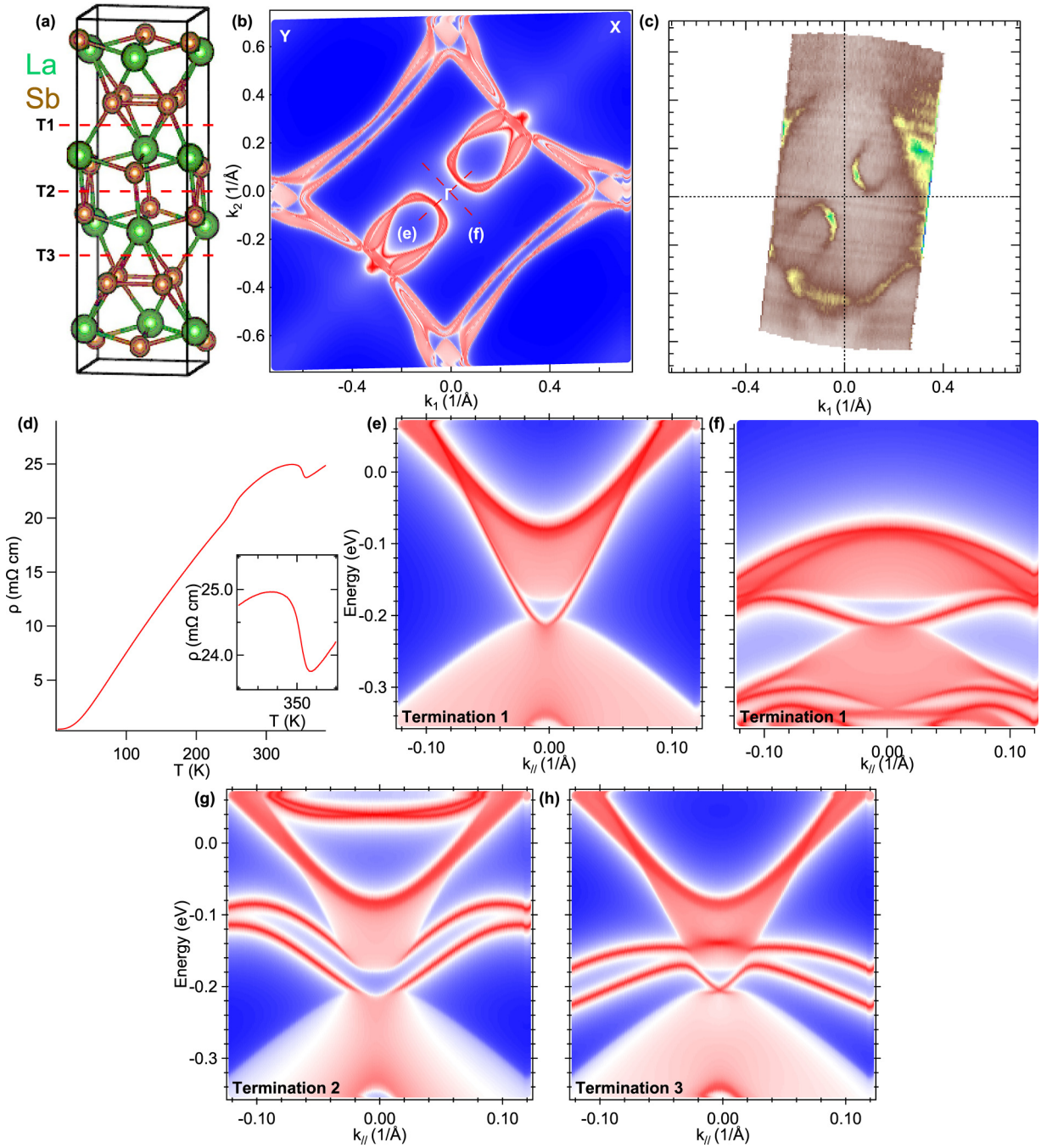

FIG. 1. Density-functional theory band-structure calculation, with predicted surface termination for $LaSb_2$. (a) Crystal structure of $LaSb_2$ arrows indicate possible termination planes. T1 is $(LaSb)_2$ termination, T2 is LaSb termination, and T3 is Sb termination. (b) Predicted Fermi surface for T1 termination, showing BZ labeling. (c) ARPES intensity at Fermi level taken at 7 K integrated within 10 meV of the Fermi cutoff. ARPES data was taken with a bias potential of −7 V applied to the sample. (d) Resistivity curve from our sample; inset shows rise in resistivity at 355 K. (e), (f) Surface spectral functions along the cuts shown in (b) for the T1 termination, compare with Figs. 2(e) and 2(h), respectively. (g), (h) Surface spectral functions for terminations T2 and T3.

dispersion. Figure 2(h) shows a cut perpendicular through Γ and shows a downwards dispersion. In Figs. 2(c)–2(g), the bottom of the band is exactly the dispersion shown in Fig. 2(h). The energy distribution curve (EDC) shown in Fig. 2(b) indicates the location of the saddle point is −0.19 eV. In Figs. 1(e) and 1(f), DFT calculations also predict the observed saddle point. Given that the saddle point occurs at a rather high binding energy, it is unlikely to be tuned to the Fermi level. It is worth recalling that the CDW was enhanced as $LaSb_2$ was doped with Ce [8]. This enhancement could potentially be an effect of the saddle point shifting lower in binding energy.

Charge density wave states occur when electrons and phonons become coupled, causing the electron density to be periodically displaced. The period of the CDW can be either commensurate or incommensurate with the period of

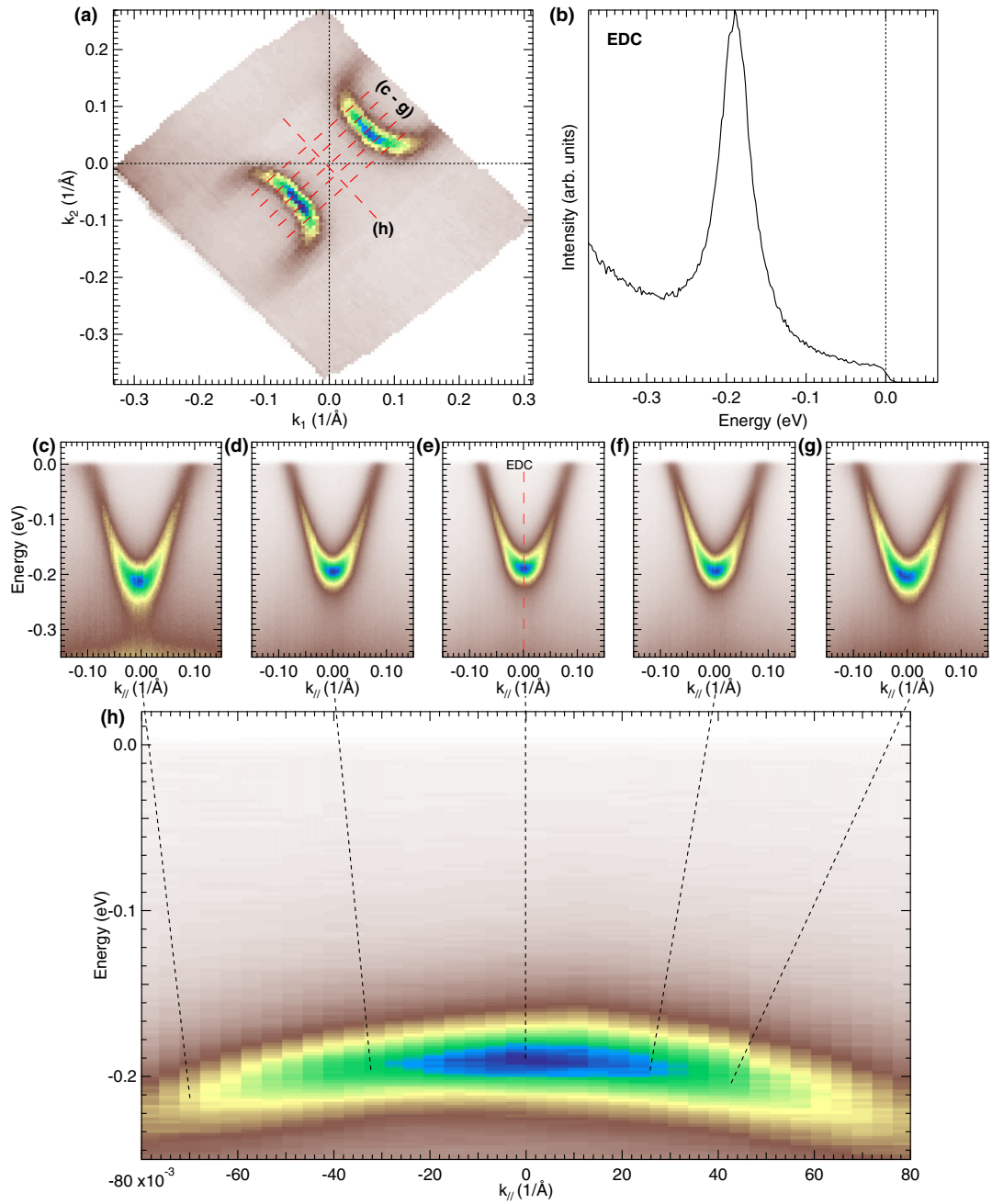

FIG. 2. ARPES data showing saddle point. (a) Map shown at 7 K integrated within 10 meV around the Fermi cutoff. (b) EDC taken at cut shown in (e) with peak indicating the location of the saddle point. (c)–(h) Energy dispersion cuts through lines in (a) showing a saddle point in the band structure.

the lattice. Both commensurate and incommensurate CDWs may potentially cause lattice distortions. This disrupts the periodicity of the lattice, leading to changes in the size and shape of the BZ and potentially causing band folding. Incommensurate CDWs may interact with impurities in the lattice, leading to a pinning of the phase of the CDW. Strong pinning can cause more pronounced affects such as lattice distortions and large frequency-dependent responses in the conductivity [42]. A CDW transition often leads to subtle or less subtle changes in the electronic structure, such as band backfolding caused by new periodicity and/or development of new energy gaps due to Fermi surface nesting like what is seen in the CDW material $2H - NbSe_2$ [43,44]. We looked carefully for these effects in the portion of the BZ accessible in our experiments.

Proposed nesting vectors predicted by DFT calculations are shown in Fig. 3(a). The lengths of the nesting vectors were determined through investigation of the electronic susceptibility, shown in Figs. 3(b) and 3(c). A peak in the electronic susceptibility may help to satisfy the Chan-Heine criterion for strong electron-phonon coupling, increasing the probability of CDW formation and Fermi surface nesting [45]. Nesting vectors connect parallel contours on the calculated Fermi surface. The predicted lengths of the nesting vectors are

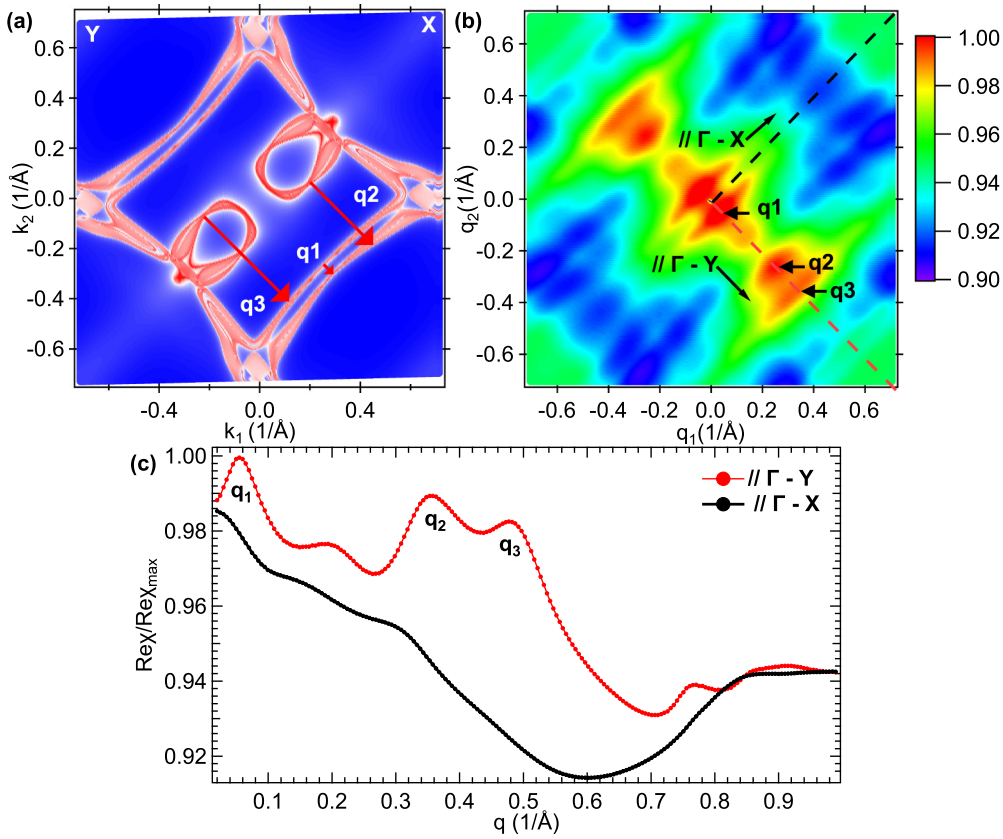

FIG. 3. Density functional theory electronic susceptibility calculation. (a) Calculated band structure at the Fermi level, with arrows indicating potential nesting vectors. (b), (c) Electronic susceptibility plotted as a function of q vector. Dotted red (black) line in (c) shows data along dashed red (black) line in (b).

$\vec{q}_1 = 0.11\ \pi/b$, $\vec{q}_2 = 0.71\ \pi/b$, and $\vec{q}_3 = 0.96\ \pi/b$, none of the predicted nesting vectors are rational fractions indicating that the CDW in $LaSb_2$ is likely incommensurate with the lattice. This conclusion aligns with the previous study showing a sharper CDW transition in Ce-doped $LaSb_2$, where they claim the introduced disorder pins the CDW [8]. The calculations are used here to provide insights on where potential effects due to the CDW might be observed in ARPES data. We note that the directions of vectors corresponding to maxima in dynamic susceptibility are orthogonal to the nesting vector reported in Ref. [12]. The intensity of the backfolded band in that study is comparable to the intensity of the primary band, which is inconsistent with the weak nature of the CDW in this material as well as our current data, where it remains below our detection limit down to lowest temperatures. Such unusually strong signal is more consistent with crystal twinning rather than signatures of CDW.

It is worth noting that no quantitative analysis was done on the Fermi surface shown in Fig. 1(c) due to the possibility of introduced distortions caused by the voltage that was applied to increase angular view of the analyzer. This data was displayed to qualitatively show more of the BZ. In Figs. 4(a)–4(c), the temperature evolution of the Fermi surface is shown. The only noticeable difference in the ARPES data through the transition is a slight shift in intensity of the spectra. This can be seen in the cuts along the X-Γ-X direction shown in Figs. 4(d)–4(f). The band appears sharper and more intense at 7 K, with high intensity at −0.19 eV. The spectrum at 330 K shows a band with the same shape to the band in the 7 K spectra, but with a much lower intensity. At 330 K, the band has slightly shifted to lower binding energy relative to its position at 7 K. The shift of the band is an effect of changing temperature, comparable to what is seen in WTe_2 [46]. In Figs. 4(g)–4(o), we examine several locations near where DFT calculations predict possible nesting vectors may form. From these data, we see no changes indicative of Fermi surface nesting. It is likely that $LaSb_2$ undergoes a transition between 7 K and 330 K [12,14]. However, we see no qualitative changes in the 7 K spectra when compared to the 330 K spectra. In Fig. 3(b), the nesting vectors $\vec{q}_2$ and $\vec{q}_3$ connect the inner pocket to the outer pockets on the Fermi surface. Though we don't see the outer pockets in Figs. 4(a)–4(c), we would expect the inner pocket to become gapped if Fermi surface nesting was occurring. No gap is observed in data shown in Figs. 4(h), 4(k) or 4(n).

Next, we closely investigated the parallel portion of the pockets near Γ. This is the location previously reported to show bandfolding under 200 K [12]. An EDC taken at the band crossing is shown in Fig. 5(c), and there is no indication of an energy gap forming when entering the CDW state. Given the high transition temperature, one would expect an energy gap to be easily detectable. We show MDCs at the Fermi level in Fig. 5(d), and again no observable changes occur when going through the CDW transition. To more precisely investigate

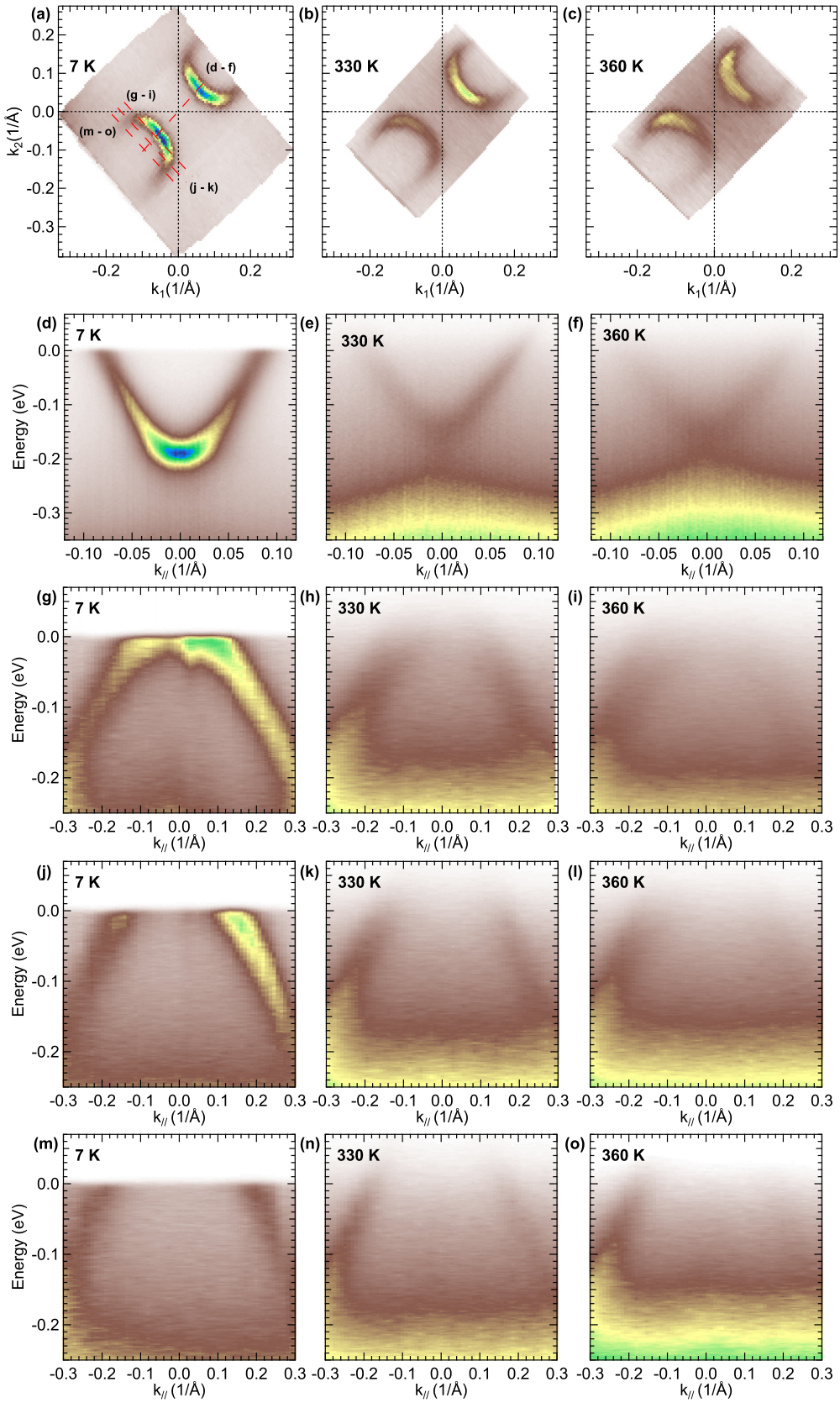

FIG. 4. ARPES intensity at the Fermi level, at several temperatures across the CDW transition. (a)–(c) Measured at 7 K, 330 K, and 360 K, respectively. (d)–(o) Band dispersion at cuts shown by red lines in (a).

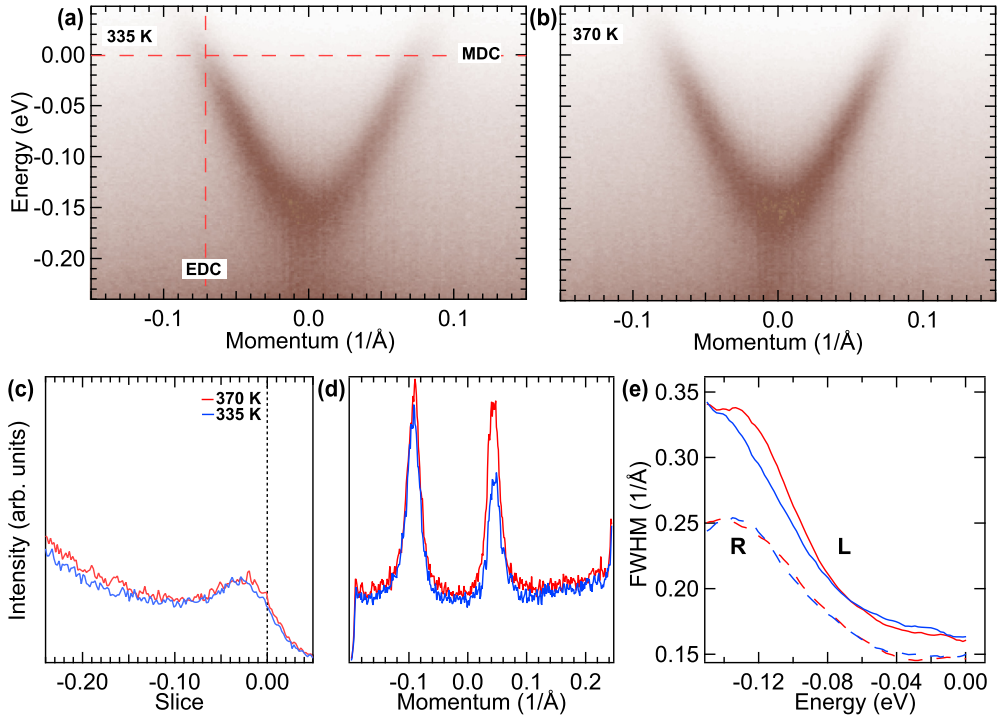

FIG. 5. Comparison of bandwidth when crossing through the CDW transition. (a), (b) Cuts taken of electron band centered at Γ, at 335 K and 370 K. (c), (d) Energy distribution curve and momentum distribution curve, respectively, through lines in (a). (e) Full width at half maximum (FWHM) of the Lorentzian fit of MDCs, solid line is FWHM of the left branch of the band, the dashed line is the right branch. Color indicates temperature.

any potential changes due to the CDW, we studied changes to the quasiparticle lifetime across the CDW transition. This was done by fitting the MDC, like the ones shown in Fig. 5(d), with Lorentzian functions for a range of binding energies. As shown in Fig. 5(e), there are no quantitative changes in the width of the electronic bands when going through the CDW transition, demonstrating that the CDW did not cause any changes in the quasiparticle lifetime in this portion of the BZ. This result aligns with a previous study showing ARPES data in the normal state above 200 K [12].

The CDW transition in $LaSb_2$ has been fairly elusive in experiments thus far. Effects seen in STM experiments on $La_{0.6}Ce_{0.4}Sb_2$ show a nesting vector of length 0.5 $Å^{-1}$. This is very comparable to $\vec{q}_3$ [8]. The introduced disorder due to the introduction of Ce into $LaSb_2$ is suspected to pin the CDW, causing the CDW transition to be more apparent. This conclusion makes sense with what we see in this study. We conclude from our data that $LaSb_2$ hosts an incommensurate CDW that is weakly pinned to the lattice. Due to the weak nature of the CDW, we see no changes in the electronic structure in the ARPES data.

IV. CONCLUSIONS

In summary, we preformed detailed ARPES measurements and DFT calculations to investigate the electronic properties of $LaSb_2$ that host high- and low-temperature CDW states. The ARPES data agrees relatively well with DFT calculations and shows a Fermi surface with two small pockets located near Γ, and four larger pockets around the edge of the BZ. These results agree with previous dHvA data, ARPES data, and DFT calculations [17,18]. No observable changes in the band structure occur when going through the CDW transitions. Indicating the weak nature of the incommensurate CDW in $LaSb_2$Å interesting feature is the presence of a saddle point predicted by DFT calculations and confirmed by our ARPES measurements. The saddle point was centered at Γ and −0.19 eV below the Fermi level. This is relatively high in binding energy, but worth investigating further through doped $LaSb_2$ compounds. Further investigation of the CDW could also be done on doped samples. We would expect from previous studies to see more of an effect by the CDW on the electronic structure in doped samples due to the introduced disorder acting as pinning centers.

ACKNOWLEDGMENTS

This work was supported by the U.S. Department of Energy, Office of Basic Energy Sciences, Division of Materials Science and Engineering, Ames National Laboratory which is operated for the U.S. Department of Energy by Iowa State University under Contract No. DE-AC02-07CH11358. L.-L.W. acknowledges support from Ames National Laboratory's LDRD.

[1] N. L. Eatough and H. T. Hall, High-pressure synthesis of rare earth diantimonides, Inorg. Chem. **8**, 1439 (1969).

[2] P. C. Canfield and Z. Fisk, Growth of single crystals from metallic fluxes, Philos. Mag. B **65**, 1117 (1992).

[3] P. C. Canfield, J. Thompson, and Z. Fisk, Novel Ce magnetism in Ce dipnictide and Di-Ce pnictide structures, J. Appl. Phys. **70**, 5992 (1991).

[4] S. L. Bud'ko, P. C. Canfield, C. H. Mielke, and A. H. Lacerda, Anisotropic magnetic properties of light rare-earth diantimonides, Phys. Rev. B **57**, 13624 (1998).

[5] S. L. Bud'ko, S. Huyan, P. Herrera-Siklody, and P. C. Canfield, Rapid suppression of charge density wave transition in $LaSb_2$ under pressure, Philos. Mag. **103**, 561 (2023).

[6] J. A. Galvis, H. Suderow, S. Vieira, S. L. Bud'ko, and P. C. Canfield, Scanning tunneling microscopy in the superconductor $LaSb_2$, Phys. Rev. B **87**, 214504 (2013).

[7] P. Ruszała, M. J. Winiarski, and M. Samsel-Czekała, Dirac-like electronic-band dispersion of $LaSb_2$ superconductor and its counterpart $LaAgSb_2$, Acta Phys. Pol. A **138**, 748 (2020).

[8] R. F. Luccas, A. Fente, J. Hanko, A. Correa-Orellana, E. Herrera, E. Climent-Pascual, J. Azpeitia, T. Pérez-Castañeda, M. R. Osorio, E. Salas-Colera, N. M. Nemes, F. J. Mompean, M. Garcia-Hernandez, J. G. Rodrigo, M. A. Ramos, I. Guillamon, S. Vieira, and H. Suderow, Charge density wave in layered $La_{1-x}Ce_xSb_2$, Phys. Rev. B **92**, 235153 (2015).

[9] C.-S. Lian, C. Si, and W. Duan, Unveiling charge-density wave, superconductivity, and their competitive nature in two-dimensional, Nano Lett. **18**, 2924 (2018).

[10] B. Sipos, A. F. Kusmartseva, A. Akrap, H. Berger, L. Forró, and E. Tutiš, From Mott state to superconductivity in 1T-TaS_2, Nat. Mater. **7**, 960 (2008).

[11] C.-S. Lian, C. Heil, X. Liu, C. Si, F. Giustino, and W. Duan, Coexistence of superconductivity with enhanced charge density wave order in the two-dimensional limit of $TaSe_2$, J. Phys. Chem. Lett. **10**, 4076 (2019).

[12] I. Palacio, J. Obando-Guevara, L. Chen, M. Nair, M. G. Barrio, E. Papalazarou, P. Le Fèvre, A. Taleb-Ibrahimi, E. G. Michel, A. Mascaraque *et al.*, Fermi surface of $LaSb_2$ and direct observation of a CDW transition, Appl. Surf. Sci. **610**, 155477 (2023).

[13] K. F. Fischer, N. Roth, and B. B. Iversen, Transport properties and crystal structure of layered $LaSb_2$, J. Appl. Phys. **125**, 045110 (2019).

[14] T. I. Weinberger, C. K. de Podesta, J. Chen, S. A. Hodgson, and F. M. Grosche, Pressure-dependent structural and electronic instabilities in $LaSb_2$, SciPost Phys. Proc. **11**, 018 (2023).

[15] J. F. DiTusa, V. Guritanu, S. Guo, D. P. Young, P. W. Adams, R. G. Goodrich, J. Y. Chan, and D. van der Marel, Optical conductivity and superconductivity in $LaSb_2$, J. Phys.: Conf. Ser. **273**, 012151 (2011).

[16] D. Young, R. Goodrich, J. DiTusa, S. Guo, P. Adams, J. Y. Chan, and D. Hall, High magnetic field sensor using $LaSb_2$, Appl. Phys. Lett. **82**, 3713 (2003).

[17] R. G. Goodrich, D. Browne, R. Kurtz, D. P. Young, J. F. DiTusa, P. W. Adams, and D. Hall, de Haas–van Alphen measurements of the electronic structure of $LaSb_2$, Phys. Rev. B **69**, 125114 (2004).

[18] A. I. Acatrinei, D. Browne, Y. Losovyj, D. Young, M. Moldovan, J. Y. Chan, P. Sprunger, and R. L. Kurtz, Angle-resolved photoemission study and first-principles calculation of the electronic structure of $LaSb_2$, J. Phys.: Condens. Matter **15**, L511 (2003).

[19] Y. X. Qiao, Z. C. Tao, F. Y. Wang, H. Wang, Z. C. Jiang, Z. T. Liu, S. Cho, F. Y. Zhang, Q. K. Meng, W. Xia *et al.*, Multiple topological nodal structure in $LaSb_2$ with large linear magnetoresistance, arXiv:2208.10437.

[20] P. C. Canfield, T. Kong, U. S. Kaluarachchi, and N. H. Jo, Use of frit-disc crucibles for routine and exploratory solution growth of single crystalline samples, Philos. Mag. **96**, 84 (2016).

[21] P. C. Canfield, LSP Industrial Ceramics, Canfield Crucible Sets, https://www.lspceramics.com/canfield-crucible-sets-2/ (2015).

[22] P. C. Canfield, New materials physics, Rep. Prog. Phys. **83**, 016501 (2020).

[23] R. Jiang, D. Mou, Y. Wu, L. Huang, C. D. McMillen, J. Kolis, H. G. Giesber III, J. J. Egan, and A. Kaminski, Tunable vacuum ultraviolet laser based spectrometer for angle resolved photoemission spectroscopy, Rev. Sci. Instrum. **85**, 033902 (2014).

[24] N. Gauthier, J. A. Sobota, H. Pfau, A. Gauthier, H. Soifer, M. D. Bachmann, I. R. Fisher, Z.-X. Shen, and P. S. Kirchmann, Expanding the momentum field of view in angle-resolved photoemission systems with hemispherical analyzers, Rev. Sci. Instrum. **92**, 123907 (2021).

[25] P. Hohenberg and W. Kohn, Inhomogeneous electron gas, Phys. Rev. **136**, B864 (1964).

[26] W. Kohn and L. J. Sham, Self-consistent equations including exchange and correlation effects, Phys. Rev. **140**, A1133 (1965).

[27] J. P. Perdew, K. Burke, and M. Ernzerhof, Generalized gradient approximation made simple, Phys. Rev. Lett. **77**, 3865 (1996).

[28] G. Kresse and J. Furthmüller, Efficient iterative schemes for *ab initio* total-energy calculations using a plane-wave basis set, Phys. Rev. B **54**, 11169 (1996).

[29] G. Kresse and J. Furthmüller, Efficiency of *ab-initio* total energy calculations for metals and semiconductors using a plane-wave basis set, Comput. Mater. Sci. **6**, 15 (1996).

[30] P. E. Blöchl, Projector augmented-wave method, Phys. Rev. B **50**, 17953 (1994).

[31] H. J. Monkhorst and J. D. Pack, Special points for Brillouin-zone integrations, Phys. Rev. B **13**, 5188 (1976).

[32] N. Marzari and D. Vanderbilt, Maximally localized generalized Wannier functions for composite energy bands, Phys. Rev. B **56**, 12847 (1997).

[33] I. Souza, N. Marzari, and D. Vanderbilt, Maximally localized Wannier functions for entangled energy bands, Phys. Rev. B **65**, 035109 (2001).

[34] N. Marzari, A. A. Mostofi, J. R. Yates, I. Souza, and D. Vanderbilt, Maximally localized Wannier functions: Theory and applications, Rev. Mod. Phys. **84**, 1419 (2012).

[35] D. H. Lee and J. D. Joannopoulos, Simple scheme for surface-band calculations. I, Phys. Rev. B **23**, 4988 (1981).

[36] D. H. Lee and J. D. Joannopoulos, Simple scheme for surface-band calculations. II. The Green's function, Phys. Rev. B **23**, 4997 (1981).

[37] M. L. Sancho, J. L. Sancho, and J. Rubio, Quick iterative scheme for the calculation of transfer matrices: Application to Mo (100), J. Phys. F **14**, 1205 (1984).

[38] M. L. Sancho, J. L. Sancho, J. L. Sancho, and J. Rubio, Highly convergent schemes for the calculation of bulk and surface Green functions, J. Phys. F **15**, 851 (1985).

[39] Q. Wu, S. Zhang, H.-F. Song, M. Troyer, and A. A. Soluyanov, WANNIERTOOLS: An open-source software package for novel topological materials, Comput. Phys. Commun. **224**, 405 (2018).

[40] J. L. McChesney, A. Bostwick, T. Ohta, T. Seyller, K. Horn, J. González, and E. Rotenberg, Extended van Hove singularity and superconducting instability in doped graphene, Phys. Rev. Lett. **104**, 136803 (2010).

[41] G. Li, A. Luican, J. M. B. Lopes dos Santos, A. H. Castro Neto, A. Reina, J. Kong, and E. Y. Andrei, Observation of van Hove singularities in twisted graphene layers, Nat. Phys. **6**, 109 (2010).

[42] G. Grüner and A. Zettl, Charge density wave conduction: A novel collective transport phenomenon in solids, Phys. Rep. **119**, 117 (1985).

[43] S. V. Borisenko, A. A. Kordyuk, V. B. Zabolotnyy, D. S. Inosov, D. Evtushinsky, B. Büchner, A. N. Yaresko, A. Varykhalov, R. Follath, W. Eberhardt, L. Patthey, and H. Berger, Two energy gaps and Fermi-surface "arcs" in $NbSe_2$, Phys. Rev. Lett. **102**, 166402 (2009).

[44] D. J. Rahn, S. Hellmann, M. Kalläne, C. Sohrt, T. K. Kim, L. Kipp, and K. Rossnagel, Gaps and kinks in the electronic structure of the superconductor $2H$-$NbSe_2$ from angle-resolved photoemission at 1 K, Phys. Rev. B **85**, 224532 (2012).

[45] Z. Xu, H. Yang, X. Song, Y. Chen, H. Yang, M. Liu, Z. Huang, Q. Zhang, J. Sun, L. Liu *et al.*, Topical review: Recent progress of charge density waves in 2D transition metal dichalcogenide-based heterojunctions and their applications, Nanotechnology **32**, 492001 (2021).

[46] Y. Wu, N. H. Jo, M. Ochi, L. Huang, D. Mou, S. L. Bud'ko, P. C. Canfield, N. Trivedi, R. Arita, and A. Kaminski, Temperature-induced Lifshitz transition in WTe_2, Phys. Rev. Lett. **115**, 166602 (2015).